

IONIZING RADIATION FROM $Z = 4 - 10$ GALAXIESALEXEI O. RAZOUMOV¹ AND JESPER SOMMER-LARSEN^{2,3}*Draft version January 21, 2010*

ABSTRACT

We compute the escape of ionizing radiation from galaxies in the redshift interval $z = 4 - 10$, i.e., during and after the epoch of reionization, using a high-resolution set of galaxies, formed in fully cosmological simulations. The simulations invoke early, energetic feedback, and the galaxies evolve into a realistic population at $z = 0$. Our galaxies cover nearly four orders of magnitude in masses ($10^{7.8} - 10^{11.5} M_{\odot}$) and more than five orders in star formation rates ($10^{-3.5} - 10^{1.7} M_{\odot} \text{ yr}^{-1}$), and we include an approximate treatment of dust absorption. We show that the source-averaged Lyman-limit escape fraction at $z = 10.4$ is close to 80% declining monotonically with time as more massive objects build up at lower redshifts. Although the amount of dust absorption is uncertain to 1 – 1.5 dex, it is tightly correlated with metallicity; we find that dust is unlikely to significantly impact the observed UV output. These results support reionization by stellar radiation from low-luminosity dwarf galaxies and are also compatible with Lyman continuum observations and theoretical predictions at $z \sim 3 - 4$.

Subject headings: galaxies: dwarf — galaxies: formation — methods: numerical — stars: formation

1. INTRODUCTION

The declining number density of quasars at redshift $z \gtrsim 2.5$ (Fan et al. 2001) points to stellar radiation as a likely source of cosmic hydrogen reionization. One of the key unknown parameters of reionization models is the escape fraction f_{esc} of ionizing photons from high-redshift galaxies. Observationally, f_{esc} is much easier to estimate at lower redshifts. In local starburst galaxies, most studies arrive at typical values $f_{\text{esc}} \lesssim 3 - 10\%$ (Leitherer et al. 1995; Hurwitz et al. 1997; Heckman et al. 2001; Bergvall et al. 2006; Grimes et al. 2007), corresponding to fairly large neutral gas covering factors with hydrogen column densities of $\gtrsim 10^{19} \text{ cm}^{-2}$ and escape of ionizing radiation through relatively few transparent holes in the interstellar medium (ISM). Starbursts in the disk of our own Galaxy feature $f_{\text{esc}} \sim 6\%$ normal to the disk (Bland-Hawthorn & Maloney 1999, 2001), a value which might be a factor of 2 – 3 lower when averaged over all directions.

There is strong evidence that the Lyman continuum (LyC) escape fraction evolves with redshift. A quantity often measured in high-redshift observations is the relative escape fraction $f_{\text{esc}}^{\text{rel}} = f_{\text{esc}}/f_{\text{esc},1500}$ defined as the ratio of the escape fraction of Lyman-limit photons f_{esc} to that of 1500\AA photons. The conversion between f_{esc} and the relative escape fractions depends on the amount of dust attenuation at 1500\AA within each galaxy and is often uncertain (Inoue et al. 2005). Large observed samples of $z \sim 1$ starburst galaxies point to fairly low $f_{\text{esc}}^{\text{rel}} \lesssim 8 - 10\%$ (Siana et al. 2007); however, the ionizing output changes toward higher redshift. At $z \sim 3$, from direct detection of LyC emission from 2 of

the 14 studied star-forming galaxies Shapley et al. (2006) put constraints on the relative escape fraction around $f_{\text{esc}}^{\text{rel}} \sim 14\%$. More recently, Iwata et al. (2009) expanded the search to 198 galaxies at $z \approx 3.1$, detecting LyC radiation from seven Lyman break galaxies (LBGs) and 10 Lyman α emitters (LAEs), estimating that prior to accounting for intergalactic medium (IGM) attenuation the average relative escape fraction is $f_{\text{esc}}^{\text{rel}} = 61\%$. Taking into account IGM attenuation with a median LyC opacity $\tau_{\text{IGM}} = 0.59$ results in $f_{\text{esc}}^{\text{rel}} = 110\%$, which in their estimate translates into the average absolute escape fraction $f_{\text{esc}} = 26\%$, and a lower limit of $f_{\text{esc}} = 15\%$ prior to accounting for IGM attenuation. Furthermore, from a comparison of direct observations of the LyC from galaxies and indirect estimates from intergalactic medium (IGM) ionization, Inoue et al. (2006) found evidence for redshift evolution of the average f_{esc} from 1 – 2% at $z = 2$ to $\sim 10\%$ at $z \gtrsim 3.6$.

Some of the first theoretical estimates of f_{esc} were derived from studies of gas distribution in the Milky Way and from analytical models of galaxy formation. Dove & Shull (1994) found $f_{\text{esc}} \sim 7\%$ for OB associations in the Galactic disk. Additional absorption comes from the shells of expanding superbubbles which further become Rayleigh-Taylor unstable, making the problem of calculating f_{esc} dependent on time and on details of star formation (Dove et al. 2000). Analytical estimates of f_{esc} in the cosmological context allowed us to study its dependence on multiple parameters, such as redshift, dark matter halo mass, baryonic fraction, star formation efficiency, and stellar ionizing output (Ricotti & Shull 2000; Wood & Loeb 2000).

More accurate theoretical constraints on f_{esc} can be derived from cosmological hydrodynamical models incorporating star formation and transfer of ionizing radiation in the surrounding gas. At very high redshifts ($z \sim 20$) estimates show that the escape fractions reflect the large masses of Population III stars and can easily approach unity (Whalen et al. 2004; Alvarez et al. 2006). In the observable, post-reionization universe, there have

¹ Institute for Computational Astrophysics, Department of Astronomy & Physics, Saint Mary's University, Halifax, NS, B3H 3C3, Canada; razoumov@ap.smu.ca

² Excellence Cluster Universe, Technische Universität München, Boltzmannstraße 2, D-85748 Garching, Germany

³ Dark Cosmology Centre, Niels Bohr Institute, University of Copenhagen, Juliane Maries Vej 30, DK-2100 Copenhagen, Denmark; jslarsen@astro.ku.dk

been several attempts to compute f_{esc} from cosmological galaxy formation models. In our earlier simulations (Razoumov & Sommer-Larsen 2006, 2007) we found that the source-averaged f_{esc} monotonically declines with redshift, from $\sim 6 - 10\%$ at $z = 3.6$ to $\sim 1 - 2\%$ at $z = 2.39$, in line with the observational findings of Inoue et al. (2006).

Gnedin et al. (2008) used a high-resolution simulation of a Lagrangian region of a $6h^{-1}\text{Mpc}$ cosmological model. The selected region corresponds to five virial radii of a Milky Way-sized galaxy and includes the Milky Way progenitor and several dozen smaller galaxies spanning two orders of magnitude in masses and star formation (SF) rates. Analyzing these galaxies at intermediate ($z = 3 - 5$) redshifts, Gnedin et al. (2008) found that the average escape fractions do not depend on redshift and tend to correlate positively with the SF rate dropping below 10^{-3} for galaxies with SF rates less than $\sim 1\text{M}_{\odot}\text{yr}^{-1}$ and dark matter masses below $\sim 10^{10.5}\text{M}_{\odot}$. Such low f_{esc} are explained by the fact that these galaxies have a relatively small gravitational pull and achieve pressure and density necessary for SF only near the midplane of a thick neutral disk. The resulting SF regions therefore tend to be embedded deep inside the opaque disk. Consequently, Gnedin et al. (2008) point out that high-redshift galaxies might be quite inefficient in emitting ionizing radiation into the IGM.

It is widely agreed that in the absence of energetic supernovae-driven outflows the increased disk density at higher redshifts $z \sim 10$ will result in very low $f_{\text{esc}} \lesssim 1\%$ for smooth disks (Wood & Loeb 2000). On the other hand, simulated galactic disks in cold dark matter (CDM) cosmologies suffer the excessive loss of angular momentum resulting in galaxies that are too small compared to observations (Fall & Efstathiou 1980). A plausible solution to this angular momentum problem is heating via feedback from stars and supernovae that would impede rapid gas cooling and collapse of small protogalactic gas clouds at high redshifts, allowing gas to preserve a larger fraction of its angular momentum as it settles into the disk. Sommer-Larsen et al. (2003) showed that a population of realistic disk, lenticular, and elliptical galaxies with almost the correct amount of angular momentum can be obtained self-consistently in cosmological simulations by invoking energetic stellar feedback at early times, either through a much higher SF efficiency than in present-day galaxies, a more top-heavy initial mass function (IMF), or both. The affected dwarf galaxies would not have time to settle into a disk in which feedback would be rather inefficient (Mac Low & Ferrara 1999). Instead, they maintain a more spherical or irregular shape resulting in a much stronger impact from stellar feedback.

Recently, using very high resolution (0.1pc) coupled radiation hydrodynamics simulations of dwarf galaxies in the mass range $10^{6.5} - 10^{9.5}\text{M}_{\odot}$ at $z = 8$, Wise & Cen (2009) showed that the time-averaged f_{esc} can reach up to 80% in halos above 10^8M_{\odot} with a top-heavy IMF, i.e., in active star-forming galaxies dominated by the atomic line cooling. It is not clear to what extent f_{esc} depends on the IMF as Wise & Cen (2009) kept the SN feedback strength equal in their normal and top-heavy IMF calculations varying only the ionizing photon production rate.

On the other hand, lower mass ($< 10^{7.5}\text{M}_{\odot}$), molecular cooling galaxies in their simulations have much lower SF efficiency and do not contribute a significant flux to reionize the universe. Irrespective of the mass of the galaxy, Wise & Cen (2009) found that f_{esc} can vary by up to an order of magnitude on the timescale of a few Myrs which is the dynamical time of a star-forming molecular cloud.

Yajima et al. (2009) also found very large escape fractions of order $20 - 60\%$ at $z = 3.7 - 7$, analyzing a very high resolution (1024^3) hydrodynamical model of a supernova-dominated primordial galaxy (Mori & Umemura 2006). However, their model is a single isolated galaxy taken out of the cosmological context.

In this paper, we take an approach complimentary to that of Wise & Cen (2009). Even though we do not have their ultra-high resolution and we solve the radiative transfer and ionization equations separately from the equations of hydrodynamics, we examine the escape of ionizing photons from a set of high-resolution reionization-epoch galaxies that evolve into a realistic population of galaxies at $z = 0$. Specifically, a two-mode SF prescription is adopted, with both the SF efficiency of the “early” mode and the feedback strength calibrated to (1) overcome the angular momentum problem (Sommer-Larsen et al. 2003), and to (2) produce a reasonable cosmic enrichment history that fits observations (Sommer-Larsen & Fynbo 2008). This efficient high- z feedback drastically changes the appearance of star-forming galaxies during the reionization era leading to much higher f_{esc} than, e.g., in $z = 3 - 5$ dwarf galaxies (Gnedin et al. 2008).

This paper is organized as follows. First, we describe our galaxy formation models and the technique to compute f_{esc} in §2. We present the results of our study including the effect of dust absorption in §3, and summarize our findings in §4.

2. MODEL

2.1. Simulated galaxies

We use an improved version of the TreeSPH code (Sommer-Larsen et al. 2003) to rerun nine galaxies selected from a larger cosmological simulation. Table 1 lists the following model parameters for each galaxy: physical box size L , circular velocity v_c at $z = 0$, mass of an SPH and a dark matter particle, and gravitational smoothing lengths for SPH and dark matter particles. The code employs the “conservative entropy” formulation (Springel & Hernquist 2002), includes star formation by conversion of SPH particles into star particles, and accounts for non-instantaneous recycling of gas and heavy elements via type II and type Ia SNe and via stellar mass loss. Chemical evolution is traced using 10 separate elements (H, He, C, N, O, Mg, Si, S, Ca, and Fe). All galaxies in Table 1 were computed with the Salpeter IMF which produces a more reasonable cosmic enrichment history than the lower metal yield Kroupa IMF (Sommer-Larsen & Fynbo 2008). Each galaxy was modeled with at least 10^6 particles. By $z = 0$ these galaxies evolve into systems with a wide range of masses, from a dwarf galaxy to a super Milky Way sized system, characteristic of the “field”. In terms of the luminosity function, they span a range from super- L^* to about $6 - 7$ magnitudes below L^* . For analysis we use outputs at

TABLE 1
LIST OF MODELED GALAXIES.

Galaxy	Box Size kpc	$v_c(z=0)$ km s^{-1}	m_{sph} $10^5 M_\odot$	m_{dm} $10^5 M_\odot$	ϵ_{sph} kpc	ϵ_{dm} kpc
S29	250	205	1.4	8.1	0.29	0.52
S33	250	180	1.4	8.1	0.29	0.52
S33sc	250	300	8.3	47	0.53	0.94
S41	250	150	1.4	8.1	0.29	0.52
S87	100	132	0.18	1.0	0.15	0.26
S108	100	131	0.18	1.0	0.15	0.26
S108sc	80	35	0.022	0.13	0.07	0.13
S115	100	125	0.18	1.0	0.15	0.26
S115sc	80	50	0.038	0.22	0.09	0.16

$z = 10.4, 8.2, 6.7, 5.7, 5.0$, and 4.4 which are separated by 200 Myrs. Fig. 1 shows the evolution of density distribution in five galaxies that cover a range of masses, and Fig. 2 displays in addition the distributions of stellar particles and heavy elements in galaxy S33.

2.2. Method

We model SF by creating discrete star “particles”, each representing a population of stars born at almost the same time in accordance with the Salpeter IMF. The stellar UV luminosity is determined using the population synthesis package Starburst 1999 (Leitherer et al. 1999) with continuous SF distributed among all stars younger than 34 Myrs. We compute the effect of this radiation on the surrounding gas with radiative transfer on top of a nested set of grids containing three-dimensional distributions of physical variables. To create such a set from the SPH simulation datasets, we projected each galaxy onto a 128^3 uniform grid, divided every base grid cell which contains more than $N_{\text{max}} = 10$ SPH particles, and continued this process of subdivision recursively so that no cell contains more than N_{max} gas particles. For the actual transport of ionizing radiation around star-forming regions, we employ the ray-tracing scheme with adaptively splitting radial rays around point sources (Abel & Wandelt 2002; Razoumov & Sommer-Larsen 2006). At each source, we start with 12 isotropic rays using HEALPix discretization on the sphere (Górski et al. 2002) which further split into leaf rays as we move away from the source or enter a spatially refined region. The local ray angular refinement level n_{ray} is increased in integer increments to satisfy the condition

$$r_{\text{max}}(n_{\text{ray}}) \geq r_{ij} 2^{l_j}, \quad (1)$$

where r_{ij} is the distance between the source i and the cell j of the grid refinement level l_j in which the photoreaction number and energy rates are computed, and the r_{max} is a monotonically increasing function chosen to ensure that at least three ray segments connect every cell in the volume to the each source. The photoreaction rates are then used iteratively to compute ionization equilibrium.

In this paper we will work only with the absolute escape fractions defined as a fraction of photons emitted by the source at a given energy that reaches the virial radius of the host galaxy. At large redshifts, star formation is not confined to a few massive galaxies; instead, it takes place in a large number of smaller galaxies scattered throughout the volume, and in many cases the concept of

a host halo becomes quite ambiguous. To overcome this problem, for each star particle we calculate its individual radius of a sphere containing 200 times the average cosmic critical density at that redshift which is effectively a local virial radius of that particle. In calculating the ionization balance, we trace all rays to the edges of the computational volume; however, f_{esc} for each source is evaluated at its individual r_{vir} . To isolate the contribution to the UVB of sources outside largest halos, we also identify the most massive halo in each volume and calculate source-averaged f_{esc} at its r_{vir} including only star particles inside this radius.

3. RESULTS

Fig. 3 shows source-averaged Lyman-limit escape fractions of all galaxies without invoking the effects of dust which will be covered in §3.1, computed both at the virial radius of the most massive galaxy and at individual r_{vir} of each source. There is a clear trend of a larger f_{esc} towards higher redshifts. Note that at $z < 4.4$ the majority of our simulated galaxies reproduce the observed gradual decline to $f_{\text{esc}} \sim 1 - 2\%$ at $z = 2.4$ (Razoumov & Sommer-Larsen 2007). Exceptions are the more massive ($v_c(z=0) > 200 \text{ km s}^{-1}$) systems S29, S33 and S33sc which form an early large disk and reach $f_{\text{esc}} < 10\%$ before $z = 4$. A very interesting result is the large escape fractions of near unity towards higher redshifts $z \sim 8 - 10$ matching the findings of Wise & Cen (2009) in globally turbulent dwarf $10^8 - 10^{10} M_\odot$ galaxies at $z = 8$. The escape fractions show an approximate inverse correlation with both the halo mass and the SF rates (Fig. 4 and Fig. 5), coinciding with the gradual increase in galaxy mass and the decline in SF efficiency with time. Note that these systems are all actively star-forming galaxies; however, their properties evolve considerably from $z = 10.4$ to 4.4 , as they move from the early efficient, self-propagating SF in turbulent, metal-poor dwarf galaxies to the late inefficient mode of SF from pre-enriched gas supplied to heavy galactic disks by smooth cooling flows (Sommer-Larsen et al. 2003).

Our lower mass ($\sim 10^8 - 10^9 M_\odot$) galaxies are still massive enough so that even at high SF rates feedback is not efficient at expelling most of the gas from the galaxy (Wise & Cen 2009) but plays an important role in shaping small-scale fluctuations in the ISM, leading to high f_{esc} . This can be seen in all our low-mass, high-SF rate galaxies all of which have fairly large f_{esc} . On the other hand, there is a significant spread in properties of individual galaxies as the escape fraction cannot be derived exclusively from the halo mass and the SF rate as demonstrated in the lower panel in Fig. 5.

LyC radiation from stars in secondary/satellite galaxies is an important contributor to the cosmic ionizing background during the early stages of galaxy assembly as evidenced by the difference between the two types of escape fractions in Fig. 3 (open and filled circles). On the other hand, in massive galaxies the overwhelming majority of star-forming regions are found inside the disks, and the two escape fractions become almost identical.

In Fig. 6, we use individual star-forming regions to derive a redshift-dependent fit $f_{\text{esc}}(M_{\text{halo}})$. Our fitting function is based on a simple toy model of the optical depth τ to the center of a uniform neutral gas sphere

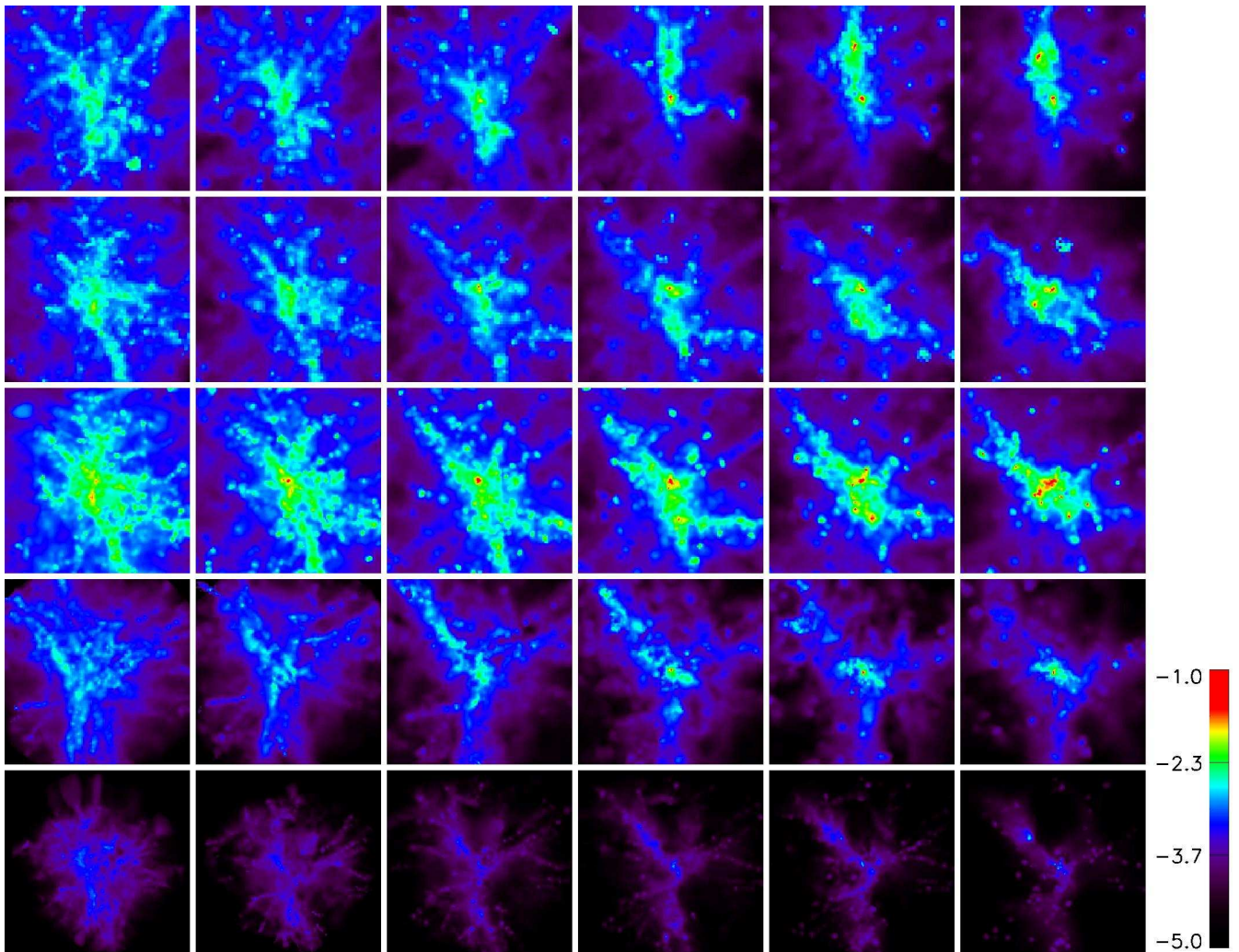


FIG. 1.— Projected gas density in galaxies S29, S33, S33sc, S108, S108sc (top to bottom), at $z = 10.4, 8.2, 6.7, 5.7, 5.0$, and 4.4 (left to right). The side of the image in each row is 125, 125, 250, 80, 80 physical kpc (top to bottom). The color scale is logarithmic from $10^{-5} \text{ g cm}^{-2}$ to $10^{-1} \text{ g cm}^{-2}$ in all images.

TABLE 2
 $f_{\text{esc}}(M_{\text{halo}})$ FITS.

z	α	β
10.4	2.78×10^{-2}	0.105
8.2	1.30×10^{-2}	0.179
6.7	5.18×10^{-3}	0.244
5.7	3.42×10^{-3}	0.262
5.0	6.68×10^{-5}	0.431
4.4	4.44×10^{-5}	0.454

inside the virial radius $\tau \propto (1+z)^2 M_{\text{halo}}^{1/3}$. We account for deviations from a uniform sphere – clumpy gas, non-uniform radial distribution, partial ionization – by introducing a second parameter with $f_{\text{esc}} = \exp(-\alpha M_{\text{halo}}^\beta)$, where α and β are functions of redshift (Table 2).

3.1. Dust absorption

We follow the prescription of Gnedin et al. (2008) to include an approximate treatment of dust absorption based on the dust extinction curve for the Small Magellanic Cloud (SMC). We use oxygen abundance as a proxy for metallicity, and assume the SMC metallicity to be 20% solar. The dust optical depth can be written

as

$$\tau_{\text{dust}}(\lambda) = l_{\text{path}} n_{\text{H}} \sigma_{0, \text{SMC}} f(\lambda) \frac{Z/Z_{\odot}}{0.2}, \quad (2)$$

where l_{path} is the physical photon path length, n_{H} is the local neutral or total hydrogen number density, for models with complete dust sublimation and no sublimation, respectively, $\sigma_{0, \text{SMC}} = 10^{-22} \text{ cm}^2$, Z/Z_{\odot} is oxygen abundance relative to solar, and $f(\lambda)$ is the parametric wavelength-dependent fit from Gnedin et al. (2008).

Fig. 7 shows our results for the two extreme cases, with and without dust sublimation, for two large and one dwarf galaxies. In the sublimation model stellar photons destroy dust, and therefore with sufficiently large escape fractions the effect of dust on ionizing radiation is nil. Only when the escape fraction is small due to accumulation of neutral hydrogen along the line of sight, we can see some small effect of dust in the sublimation model, e.g. in the massive galaxy S33sc at $z = 5$, where the relative effect of dust is below 0.2%. Its impact is more noticeable in the no-sublimation model. The true escape fractions probably lie in between these values, as some amount of dust is likely to be destroyed by ionizing radi-

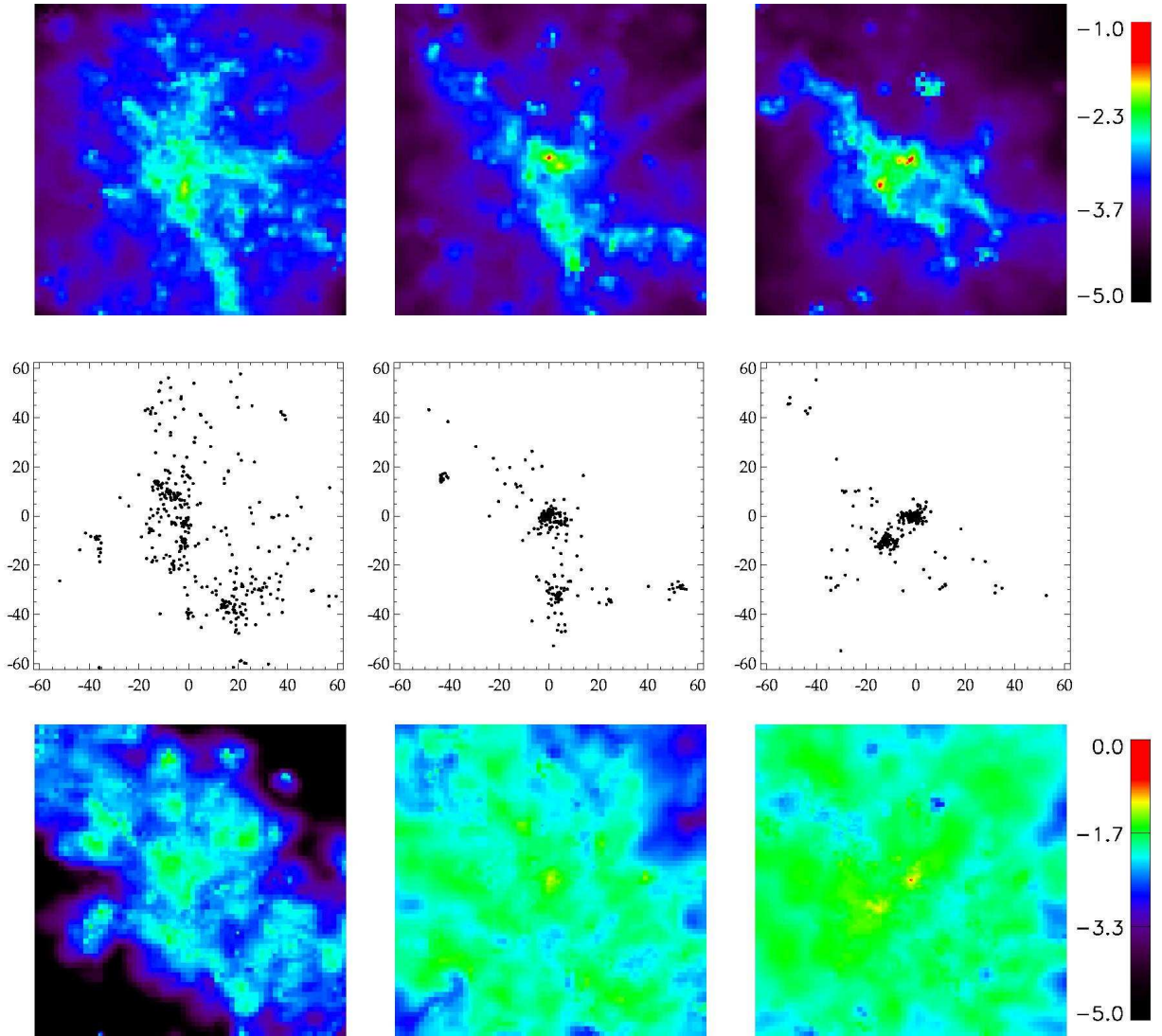


FIG. 2.— Projected gas density (top panel), stellar particle distribution (center panel), and projected mass-weighted oxygen abundance $[O/H]$ (solar units) in galaxy S33 at $z = 10.4$, 5.7 , and 4.4 (left to right). Each image is 125 physical kpc on a side. Both color scales are to the base-10 logarithm, and column density in the top panel is measured in g cm^{-2} .

ation. Similar to Gnedin et al. (2008), we find that the overall effect of dust is not very large, reducing the escape fractions by few percent at most, explained by the simple fact that photoionization of neutral hydrogen dominates the optical depths. Large escape fractions are only observed at low hydrogen column densities, where dust absorption is usually small. Its effect on the escape of ionizing radiation is more noticeable in massive galaxies at lower redshifts in which the buildup of heavy elements leads to relatively high dust concentrations (Fig. 7).

It is worth pointing out that the magnitude of dust absorption is highly uncertain and can range significantly in different studies. Recently, Yajima et al. (2009) suggested another simple model of calculating τ_{dust} from chemical composition under the following assumptions: (1) absorption is caused by dust grains ranging in radius from $0.1 \mu\text{m}$ to $10 \mu\text{m}$; (2) the size distribution of dust grains scales as $r_d^{-3.5}$; (3) the density inside dust grains is constant at 3 g cm^{-3} ; (4) the diffraction effects are negligible since $r_d > 912 \text{ \AA}$; and (5) the mass density of dust is $0.01 Z/Z_\odot \rho_{\text{gas}}$. The resulting dust absorp-

tion is proportional to the total gas density, similar to the no-sublimation model of Gnedin et al. (2008), but is approximately 25 times weaker than the latter. Despite such low cross-sections, Yajima et al. (2009) find that the escape fractions are significantly regulated by interstellar dust in their isolated supernova-dominated galaxy. The reason for such a large effect is their relatively strong metal enrichment producing on average solar metallicity ISM at $z = 3.7$ (Fig. 8) which in addition is very irregular and moderately optically thin for ionizing photons.

Observations of UV-selected star-forming galaxies at $z \sim 2$ point to metallicities in the range $0.1\text{--}0.5$ dex below solar (Erb et al. 2006). If star formation peaks at $z \sim 2 - 3$, metallicities should be substantially lower in the interval $z \sim 10.4 - 4.4$ we study here. All models in our set feature a gradual metal enrichment such that most of the massive galaxies have $[O/H] \sim 0.1 - 0.5$ at $z = 2$ (Fig. 8). Since the no-sublimation models put an upper limit on dust absorption (Fig. 7), we conclude that its effect is unlikely to significantly impact the output of ionizing photons in $z \gtrsim 4.4$ galaxies, except for very rare,

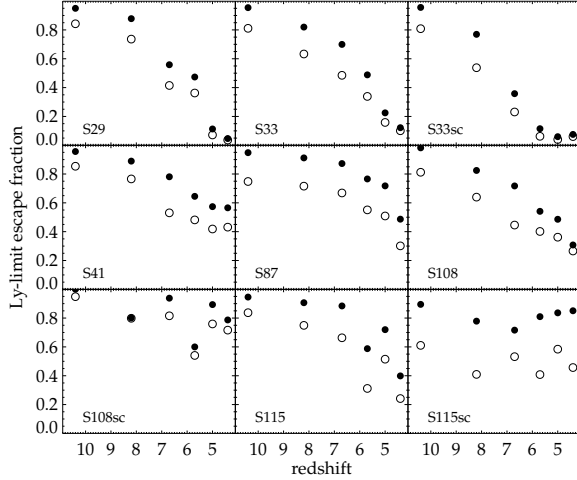


FIG. 3.— Source-averaged Lyman-limit escape fractions computed at r_{vir} of the most massive halo in each volume (open circles) and at individual r_{vir} of each star particle (filled circles) vs. redshift for the nine galaxies. The effects of dust are not included in this plot.

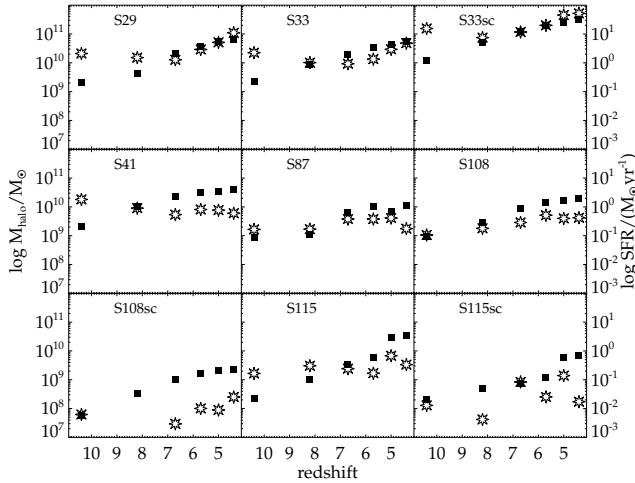


FIG. 4.— Dark matter halo masses M_{halo} (filled squares) and star formation rates (star symbols) vs. redshift for the nine galaxies.

unusually massive systems.

3.2. Resolution effects

For the numerical convergence study, we use an additional model K33 to compare the escape fractions at $z = 5.85$ obtained at standard (K33-64) and 8 times the mass resolution (K33-512), while keeping the strength of stellar feedback and the ionizing luminosity per unit stellar mass constant. At these two resolutions, this galaxy contains 755 star particles of mass $1.42 \times 10^5 M_{\odot}$, and 8447 star particles of mass $1.78 \times 10^4 M_{\odot}$, respectively.

We find the Lyman-limit $f_{\text{esc}} = (0.142, 0.118, 0.101)$ for K33-64, and $(0.215, 0.173, 0.143)$ for K33-512, at $r = (0.5, 1, 2) \times r_{\text{vir}}$, respectively (Fig. 9). The star formation rate in the higher resolution model is slightly larger, $4.4 M_{\odot} \text{ yr}^{-1}$ versus $3.2 M_{\odot} \text{ yr}^{-1}$, which could explain the observed difference in f_{esc} , since the two quantities should be coupled (Wise & Cen 2009). In addition,

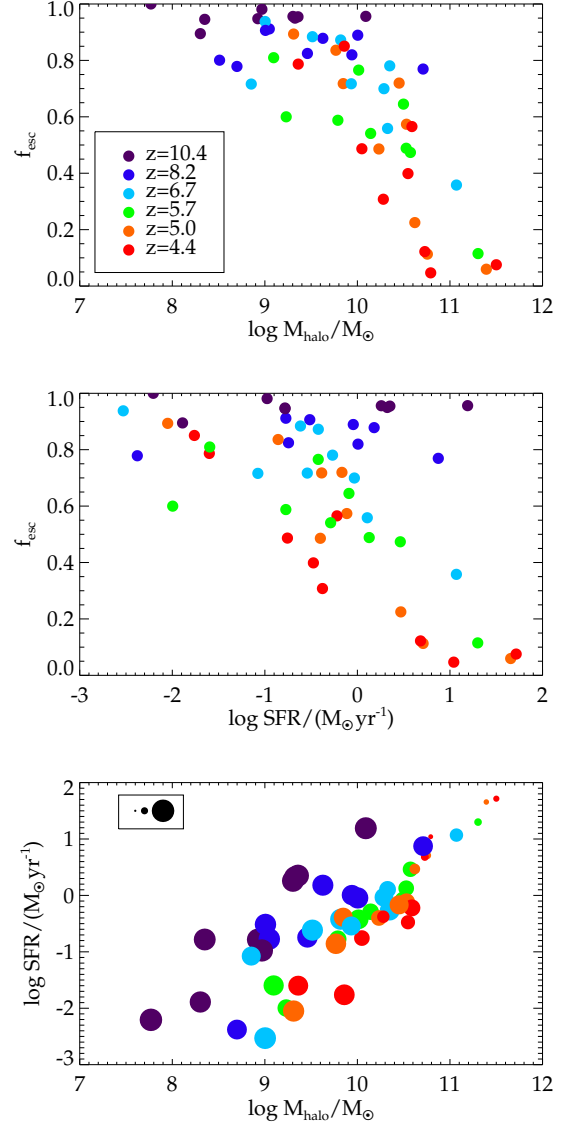


FIG. 5.— Angular averaged escape fraction as a function of the host halo mass (top) and the SF rate (center). Bottom: escape fractions in the $\log(\text{SFR}) - \log(M_{\text{halo}})$ plane, with the radius of each circle proportional to $f_{\text{esc}}^{0.5}$. The insert box in the bottom panel shows $f_{\text{esc}} = 10^{-2}$, 10^{-1} , and 1. Color in all three panels represents redshift with the rainbow palette, from $z = 10.4$ (violet) to $z = 4.4$ (red).

we see the increased porosity of the ISM in the higher resolution model, with more transparent channels between dense clumps through which radiation can escape. To be conservative, the escape fractions presented in this work should probably be considered as lower limits.

4. DISCUSSION AND CONCLUSIONS

We have coupled high-resolution galaxy formation models with point-source radiative transfer to compute the escape fractions of LyC photons from galaxies at $z = 10.4, 8.2, 6.7, 5.7, 5.0$, and 4.4 . We confirm very large escape fractions of near unity at $z \sim 8 - 10$ found by Wise & Cen (2009) in dwarf $10^8 - 10^{10} M_{\odot}$ galaxies, conducive to efficient stellar reionization. The difference between this result and much lower escape fractions in $M_{\text{halo}} \gtrsim 8 \times 10^9 M_{\odot}$ galaxies with similar SF rates at

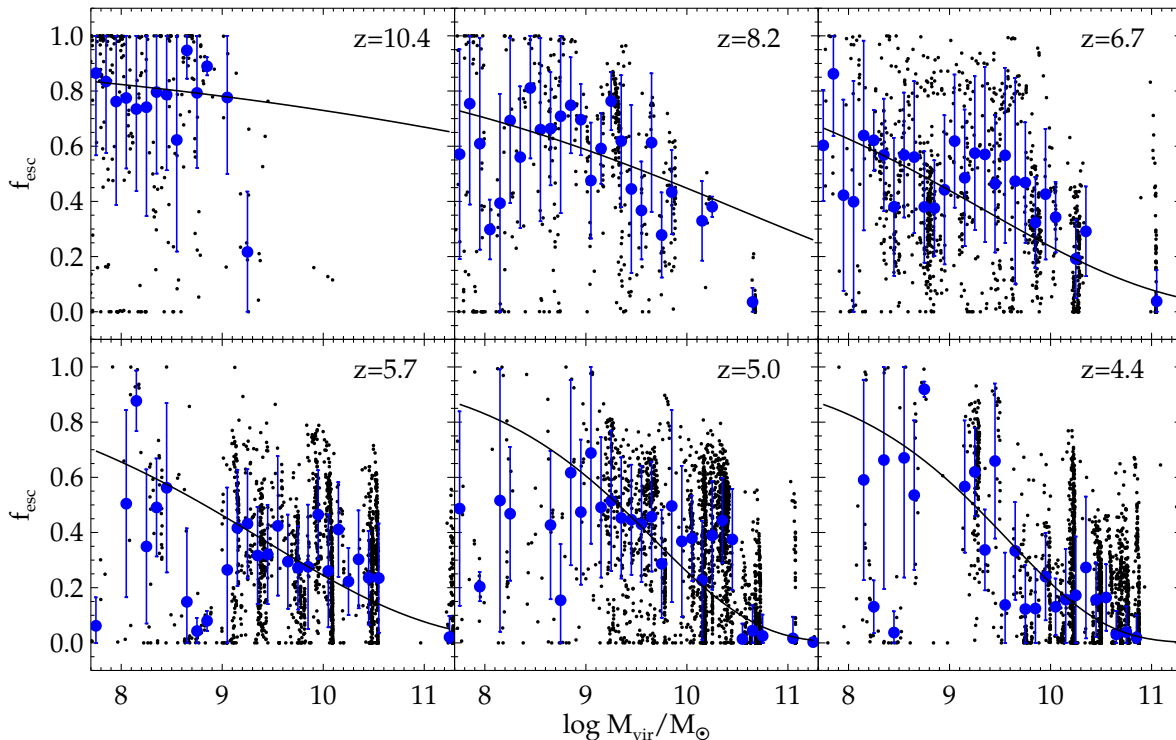


FIG. 6.— The Lyman-limit escape fractions of all star-forming regions (black dots) in all modeled galaxies vs. the host halo mass $M(r_{\text{vir}}, z)$ at six redshifts, computed at individual r_{vir} of each star particle. The blue circles and the error bars show f_{esc} averaged inside each mass bin, along with standard deviations. The lines show redshift-dependent two-parameter exponential fits (see the text for details).

$z = 3 - 4$ (Gnedin et al. 2008) reflects the model differences between reionization-epoch star-forming galaxies and lower-redshift dwarf galaxies with a relatively low SF efficiency. There are several physical factors that could account for very different SF efficiencies in $z \sim 6 - 10$ galaxies. These systems are likely to have very low metallicities for which the strength of stellar winds is greatly reduced (Kudritzki 2002), producing less local disruption in star-forming clouds, and leading to higher SF efficiency. Lower metallicities correspond to less efficient cooling; however, this effect can be offset by the fact that – at a fixed halo mass – higher redshift galaxies are more compact resulting in more efficient cooling. In addition, there are theoretical expectations of a more top-heavy IMF at high redshifts (Abel et al. 2002; Bromm et al. 2002; Padoan & Nordlund 2002). A larger fraction of massive stars is likely to yield more efficient feedback on galactic scales, producing a larger number of transparent channels in the ISM through which ionizing radiation can escape the galaxy.

All our systems are proto-spiral galaxies residing in a “field” environment. We did not consider more crowded proto-elliptical environments in which evolution is accelerated due to the higher overdensity. In such galaxies the UV escape fractions could drop quicker with time than what is seen in our current study. In addition, higher metallicity might amplify the effect of dust although relatively few UV photons would escape from such environments. We will address more crowded systems in a future study.

We did not compute the effect of ionizing radiation on the hydrodynamical flow which is instead shaped by the

thermal feedback energy. Would our results change if we used a coupled radiation-hydrodynamics approach? Ionizing radiation heats up the gas which can then expand and leave the star-forming region. Gnedin et al. (2008) found overall that coupling of radiative transfer and hydrodynamics does not produce a large change in f_{esc} . For the dwarf galaxies considered by Wise & Cen (2009), they reported fast variations of f_{esc} by up to an order of magnitude on the timescale of a few Myrs which is the dynamical timescale of a star-forming molecular cloud. These changes in f_{esc} are attributed to gas expulsion by winds and supernovae creating transparent channels for ionizing photons. Since feedback by winds and supernovae is already a key part of our hydrodynamical calculations, we argue that our postprocessing of fixed time snapshots of galaxies with radiative transfer with the assumption of ionization equilibrium gives a fairly accurate estimate of the escape fractions. On the other hand, we cannot compute f_{esc} variations on short timescales of few Myrs, and therefore we cannot tell exactly how representative our computed f_{esc} of the time-average escape fractions, something we are hoping to address in the future.

The other possible source of uncertainty in computing f_{esc} is gas clumping on sub-resolution scales. Since for fixed cloud mass and ionization the optical depth scales as R^{-2} with the cloud radius R , and recombinations are more efficient at higher densities, the true f_{esc} could be smaller than our current estimates. On the other hand, star-forming clouds are shaped by feedback, and the simple $\tau \propto R^{-2}$ scaling might not be valid. Moreover, higher grid resolution would yield a more porous ISM, with a

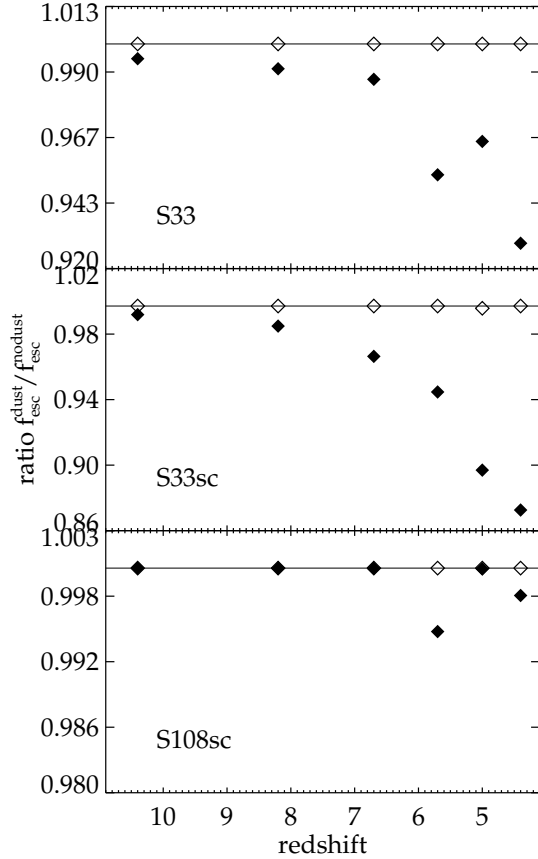


FIG. 7.— Ratio of Lyman-limit escape fractions with complete dust sublimation (open diamonds) and no sublimation (filled diamonds) to the escape fractions without dust for two large galaxies (top two panels) and a dwarf galaxy (bottom panel), as a function of redshift. The solid lines correspond to the ratio of unity.

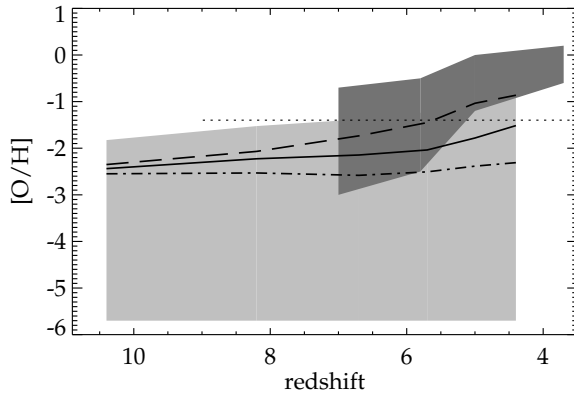


FIG. 8.— Solid, long-dashed and dash-dotted lines show mass-weighted oxygen abundance (relative to solar) in galaxies S33, S33sc, and S108sc as functions of redshift. The light-shaded area represents the range of $[O/H]$ containing 90% of the gas mass in S33, i.e., 5% of the gas has metal enrichment above and below this region. The dark-shaded area shows the range of $[O/H]$ in the supernova-dominated galaxy from Yajima et al. (2009), and the dotted horizontal line corresponds to metallicity adopted in Gnedin et al. (2008).

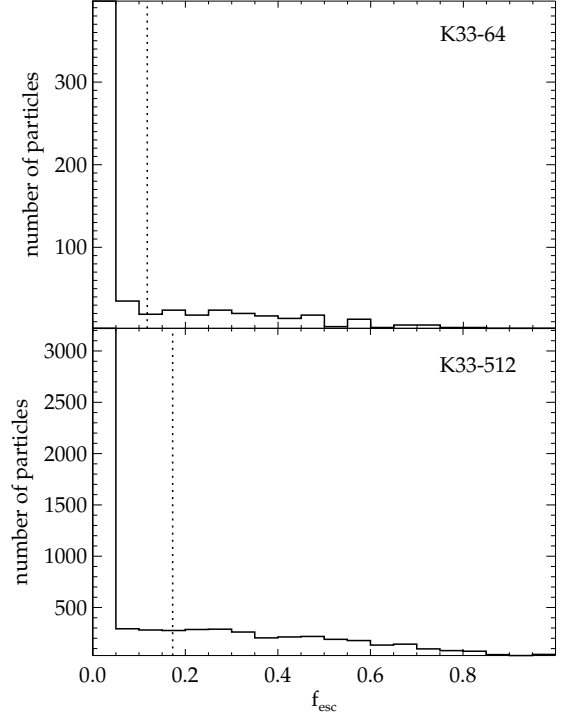


FIG. 9.— Distribution of star particles by their Lyman-limit f_{esc} at individual particle's r_{vir} at two different numerical resolutions at $z = 5.85$. The dashed lines show source-averaged f_{esc} .

strong network of transparent channels through which radiation can escape.

ACKNOWLEDGMENTS

We thank Nick Gnedin for providing his convenient parametrization of dust extinction, and the anonymous referee for many useful comments. Computational facilities for this work were provided by ACEnet, the regional high performance computing consortium for universities in Atlantic Canada. We also gratefully acknowledge abundant access to the computing facilities provided by the Danish Centre for Scientific Computing (DCSC). ACEnet is funded by the Canada Foundation for Innovation (CFI), the Atlantic Canada Opportunities Agency (ACOA), and the provinces of Newfoundland & Labrador, Nova Scotia, and New Brunswick. AR acknowledges financial support from ACEnet. This work was supported in part by the DFG Cluster of Excellence "Origin and Structure of the Universe". The Dark Cosmology Centre is funded by the Danish National Re-

REFERENCES

- Abel, T., Bryan, G. L., & Norman, M. L. 2002, *Science*, 295, 93
 Abel, T. & Wandelt, B. D. 2002, *MNRAS*, 330, L53

- Alvarez, M. A., Bromm, V., & Shapiro, P. R. 2006, *ApJ*, 639, 621
- Bergvall, N., Zackrisson, E., Andersson, B.-G., Arnberg, D., Masegosa, J., & Östlin, G. 2006, *A&A*, 448, 513
- Bland-Hawthorn, J. & Maloney, P. R. 1999, *ApJ*, 510, L33
- , 2001, *ApJ*, 550, L231
- Bromm, V., Coppi, P. S., & Larson, R. B. 2002, *ApJ*, 564, 23
- Dove, J. B. & Shull, J. M. 1994, *ApJ*, 430, 222
- Dove, J. B., Shull, J. M., & Ferrara, A. 2000, *ApJ*, 531, 846
- Erb, D. K., Shapley, A. E., Pettini, M., Steidel, C. C., Reddy, N. A., & Adelberger, K. L. 2006, *ApJ*, 644, 813
- Fall, S. M. & Efstathiou, G. 1980, *MNRAS*, 193, 189
- Fan, X., Strauss, M. A., Schneider, D. P., Gunn, J. E., Lupton, R. H., Becker, R. H., Davis, M., Newman, J. A., Richards, G. T., White, R. L., Anderson, Jr., J. E., Annis, J., Bahcall, N. A., Brunner, R. J., Csabai, I., Hennessy, G. S., Hindsley, R. B., Fukugita, M., Kunszt, P. Z., Ivezić, Z., Knapp, G. R., McKay, T. A., Munn, J. A., Pier, J. R., Szalay, A. S., & York, D. G. 2001, *AJ*, 121, 54
- Gnedin, N. Y., Kravtsov, A. V., & Chen, H.-W. 2008, *ApJ*, 672, 765
- Górski, K. M., Banday, A. J., Hivon, E., & Wandelt, B. D. 2002, in *ASP Conf. Ser. 281: Astronomical Data Analysis Software and Systems XI*, ed. D. A. Bohlender, D. Durand, & T. H. Handley, 107
- Grimes, J. P., Heckman, T., Strickland, D., Dixon, W. V., Sembach, K., Overzier, R., Hoopes, C., Aloisi, A., & Ptak, A. 2007, *ApJ*, 668, 891
- Heckman, T. M., Sembach, K. R., Meurer, G. R., Leitherer, C., Calzetti, D., & Martin, C. L. 2001, *ApJ*, 558, 56
- Hurwitz, M., Jelinsky, P., & Dixon, W. V. D. 1997, *ApJ*, 481, L31+
- Inoue, A. K., Iwata, I., Deharveng, J., Buat, V., & Burgarella, D. 2005, *A&A*, 435, 471
- Inoue, A. K., Iwata, I., & Deharveng, J.-M. 2006, *MNRAS*, 371, L1
- Iwata, I., Inoue, A. K., Matsuda, Y., Furusawa, H., Hayashino, T., Kousai, K., Akiyama, M., Yamada, T., Burgarella, D., & Deharveng, J. 2009, *ApJ*, 692, 1287
- Kudritzki, R. P. 2002, *ApJ*, 577, 389
- Leitherer, C., Ferguson, H. C., Heckman, T. M., & Lowenthal, J. D. 1995, *ApJ*, 454, L19+
- Leitherer, C., Schaerer, D., Goldader, J. D., Delgado, R. M. G., Robert, C., Kune, D. F., de Mello, D. F., Devost, D., & Heckman, T. M. 1999, *ApJS*, 123, 3
- Mac Low, M.-M. & Ferrara, A. 1999, *ApJ*, 513, 142
- Mori, M. & Umemura, M. 2006, *Nature*, 440, 644
- Padoan, P. & Nordlund, Å. 2002, *ApJ*, 576, 870
- Razoumov, A. O. & Sommer-Larsen, J. 2006, *ApJ*, 651, L89
- , 2007, *ApJ*, 668, 674
- Ricotti, M. & Shull, J. M. 2000, *ApJ*, 542, 548
- Shapley, A. E., Steidel, C. C., Pettini, M., Adelberger, K. L., & Erb, D. K. 2006, *ApJ*, 651, 688
- Siana, B., Teplitz, H. I., Colbert, J., Ferguson, H. C., Dickinson, M., Brown, T. M., Conselice, C. J., de Mello, D. F., Gardner, J. P., Giavalisco, M., & Menanteau, F. 2007, *ApJ*, 668, 62
- Sommer-Larsen, J. & Fynbo, J. P. U. 2008, *MNRAS*, 385, 3
- Sommer-Larsen, J., Götz, M., & Portinari, L. 2003, *ApJ*, 596, 47
- Springel, V. & Hernquist, L. 2002, *MNRAS*, 333, 649
- Whalen, D., Abel, T., & Norman, M. L. 2004, *ApJ*, 610, 14
- Wise, J. H. & Cen, R. 2009, *ApJ*, 693, 984
- Wood, K. & Loeb, A. 2000, *ApJ*, 545, 86
- Yajima, H., Umemura, M., Mori, M., & Nakamoto, T. 2009, *MNRAS*, 398, 715